

A quantum implementation of high-order power method for estimating geometric entanglement of pure states

Andrii Semenov¹, Niall Murphy¹, Simone Patscheider²,
Alessandra Bernardi², Elena Blokhina^{1,3}

¹Equal1 Labs, Dublin, Ireland.

²Department of Mathematics, University of Trento, Trento, Italy.

³School of Electrical & Electronic Engineering, University College
Dublin, Ireland.

Entanglement is one of the fundamental properties of a quantum state and is a crucial differentiator between classical and quantum computation. There are many ways to define entanglement and its measure, depending on the problem or application under consideration. Each of these measures may be computed or approximated by multiple methods. However, hardly any of these methods can be run on near-term quantum hardware. This work presents a quantum adaptation of the iterative higher-order power method for estimating the geometric measure of entanglement of multi-qubit pure states using rank-1 tensor approximation. This method is executable on current (hybrid) quantum hardware and does not depend on quantum memory. We study the effect of noise on the algorithm using a simple theoretical model based on the standard depolarising channel. This model allows us to *post hoc* mitigate the effects of noise on the results of the computation.

1 Introduction

For a quantum algorithm to have an advantage over a classical alternative, entanglement [1] is a necessary ingredient. Not only the presence, but the “degree” of entanglement in a quantum state is an important property for many applications [2], for example quantum information technologies [3], quantum teleportation and quantum communication [1] and quantum cryptography [4]. On the one hand, if there is not “enough” entanglement, a quantum circuit can be efficiently simulated by classical

devices [5]. On the other hand, some systems with “maximally” entangled states, such as stabiliser codes [6], admit efficient classical simulations [7, 8]. In addition, highly entangled states are not useful as computational resources in the measurement-based computing paradigm [9]. In the setting of parameterised quantum circuits, entanglement contributes to “barren plateaus” in the cost function landscape that make training a challenge [10, 11].

Consequently, there has been an effort to define and quantify [2] entanglement, with different methods [12] being preferred depending on the application. Some definitions (for example, quantum mutual information or von Neumann entropy [1]) are measures of bipartite entanglement only and are computationally expensive for mixed states. Others, such as concurrence [13], have no unique definition for higher (> 2) dimensional systems [14, 15]. In fact, the very concept of n -partite (multi-qubit) entanglement is still not clearly understood [16].

The geometric measure of entanglement (E_G) [17, 18, 19] is a popular multipartite entanglement metric with a clear geometric interpretation, which naturally extends to the n -partite case and to mixed states [19]. Geometric entanglement is, among other applications, useful when defining entanglement witnesses [19] which are used as a positive indicator of entanglement for a subset of quantum states.

The first algorithm to compute E_G used it (under the name of “the Groverian measure of entanglement”) to assess the probability of success for an initial state in Grover’s algorithm [20, 21]. This method was rephrased in terms of eigenvalues and Singular Value Decomposition (SVD) and extended to mixed states [22]. A similar method was formulated in terms of Tucker decomposition [23] using the Higher Order Orthogonal Iteration (HOOI) algorithm [24]. A parallel strand of work [25, 26], based on the fundamental connection between geometric entanglement and tensor theory, introduced a series of algorithms to approximate E_G [27, 28, 29]. These approaches can be considered as generalisations of the popular power methods (e.g. the Lanczos method and Arnoldi iterations) used to study the eigenvalues of matrices (for example, see [30]).

With accessible quantum hardware, measuring entanglement on a physical device becomes a problem of interest. The algorithms mentioned above are all intended to be executed on classical machines. Naïvely, we would have to do full-state tomography to reconstruct the quantum state in a classical computer to calculate its entanglement. As the number of qubits increases, the number of measurements required for tomography increases exponentially. Alternatively, if we know the quantum state in advance, we can prepare the appropriate entanglement witness [3]. However, the latter method does not allow one to obtain the measure of entanglement itself. Recently, variational quantum circuits (VQC) have been suggested to compute geometric entanglement of pure states on a quantum computer [31, 32]. VQC algorithms, unfortunately, suffer from “barren plateaus” [10, 11] which hinders the scalability of the approach.

In this paper, we present an iterative quantum algorithm for computing the geometric entanglement of pure quantum states. The algorithm is a quantum adaptation of the Higher Order Power Method (HOPM) [24] to find solutions for Rank-1 Tensor Approximation (RTA). We show how to implement crucial steps of HOPM in

the quantum domain and analyse their robustness w.r.t. noise. Our aim is to measure entanglement on near-term quantum devices more time efficiently than full-state tomography and more space efficiently (qubits versus classical memory) than executing HOPM on a classical device.

Our paper is structured as follows. First, we formally define geometric entanglement and its connection to RTA and recall the HOPM algorithm for this problem. Next, we present our quantum implementation of HOPM. Then we show some simulation results exploring the robustness of the algorithm to noise and discuss some simple ways to mitigate it. Finally, we discuss some future directions and unresolved questions.

2 Results

2.1 Preliminaries: Geometric Entanglement in terms of rank-1 tensor approximation

Definition 1 (Fully separable and entangled states). *Let \mathbb{H}^n be an n -qubit Hilbert space. A pure n -partite state $|\phi\rangle \in \mathbb{H}^n$ is fully separable if and only if it is a product state of 1-qubit states $|\mathbf{v}_i\rangle \in \mathbb{H}$ [1]:*

$$|\phi\rangle = |\mathbf{v}_1\rangle \otimes \cdots \otimes |\mathbf{v}_n\rangle. \quad (1)$$

We say an n -partite pure state is entangled if it is not fully separable. Let $S_n \subseteq \mathbb{H}^n$ denote the set of fully separable states.

Definition 2 (Geometric measure of entanglement [17, 18, 19]). *Let the geometric measure of entanglement of a pure state $|\psi\rangle$ be*

$$\hat{E}_G(|\psi\rangle) = 1 - \max_{|\phi\rangle \in S_n} |\langle \phi | \psi \rangle|^2, \quad (2)$$

where $\hat{\lambda} = \max_{|\phi\rangle \in S_n} |\langle \phi | \psi \rangle|$ is called the entanglement eigenvalue.

One approach to compute the value of $\hat{\lambda}$ is to solve the problem of finding the “closest” fully separable state $|\phi\rangle$ to the state $|\psi\rangle$. The closest separable state is formally stated as a minimization problem over $|\phi\rangle \in S_n$ with the objective function being the distance between $|\psi\rangle$ and $|\phi\rangle$:

$$\min_{|\phi\rangle \in S_n} d(|\psi\rangle, |\phi\rangle), \quad (3)$$

where $d(a, b) = \|a - b\|_F$ is the reference distance with $a, b \in \mathbb{H}^n$ and $\|\cdot\|_F$ being the Frobenius norm (we will omit the subscript F in what follows). We note that the minimiser of Eq. (3) exists (but may not be unique) since the set of fully separable states S_n is the classical Segre variety [33, 34, 35], which is closed in Zariski and Euclidean topology when defined over the complex numbers. Minimizing the distance from a variety is a problem well studied from different perspectives, for example in

the context of algebraic geometry the concept of Euclidean Distance Degree has been introduced [36]. In the present work we deal with the minimization of Eq. (3) in terms of a system of nonlinear equations with λ being a Lagrange multiplier (see [26, 19, 29]):

$$\begin{aligned} T_\psi \times_i (\mathbf{v}_1^*, \dots, \mathbf{v}_{i-1}^*, \mathbf{v}_{i+1}^*, \dots, \mathbf{v}_n^*) &= \lambda \mathbf{v}_i, \\ T_\psi^* \times_i (\mathbf{v}_1, \dots, \mathbf{v}_{i-1}, \mathbf{v}_{i+1}, \dots, \mathbf{v}_n) &= \lambda \mathbf{v}_i^*, \\ \|\mathbf{v}_i\|^2 = \sum_{b_i} |v_{i,b_i}|^2 &= 1, \quad i \in \{1, \dots, n\}, \quad \lambda \in \mathbb{R}, \end{aligned} \tag{4}$$

where $T_\psi \in \mathbb{C}_2^{\otimes n}$ ($\mathbb{C}_2 = \mathbb{C} \times \mathbb{C}$ is a two-dimensional complex vector space) is a tensor representation of $|\psi\rangle$ in the basis $|b_1, \dots, b_n\rangle = \otimes_i |b_i\rangle$ with components $\psi_{b_1, \dots, b_n} \in \mathbb{C}$ defined as:

$$|\psi\rangle = \sum_{b_1, \dots, b_n} \psi_{b_1, \dots, b_n} |b_1, \dots, b_n\rangle,$$

and $\mathbf{v}_i = (v_{i,0}, v_{i,1})^T \in \mathbb{C}_2$ is a vector of components of the one-qubit states $|\mathbf{v}_i\rangle$, defined in Eq. (1), in the same basis; the asterisk means complex conjugate; the symbol \times_i is n -mode vector product over all modes except the i -th one, which is a contraction of a tensor on the left with the tuple of vectors on the right, skipping the i -th index (mode) of the tensor (when the subscript is not given none of the modes are skipped). In tensor analysis, the problem of finding a solution to a system of equations such as Eq. (4) is usually referred to as the U -eigenpair problem for the tensor T_ψ . One way to solve this problem is by reducing it to RTA [26, 29].

The problem of RTA is NP-hard [37] and so exact or global techniques such as homotopy continuation methods [38] may take exponential time. Alternatively, approximate techniques may run quickly, but may return a local minima. Some of the well-known algorithms that can be used for approximating RTA are Higher-Order Singular Value Decomposition (HOSVD) [39], HOPM and HOOI [24]. In the particular case of tensors representing the pure quantum state of a finite system of qubits, both HOSVD and HOOI simplify to the HOPM algorithm, which is based upon the Alternating Least Squares (ALS) approach [24, 40] for solving non-linear systems of equations.

The application of HOPM to the first sub-system of equations in Eq. (4) is presented in pseudocode in Algorithm 1. (Note, that this is a known technique [24, 22, 26, 28, 29]).

Remark 3. *The global phase of $|\mathbf{v}_i\rangle$ and the chosen computational basis do not affect the result for λ and convergence of Algorithm 1.*

Indeed from line 8 of Algorithm 1 it is evident that global phase prefactors $e^{i\alpha_j}$ ($\alpha_j \in \mathbb{R}$) of $\mathbf{v}_j^{(k)}$ do not affect the result λ of the algorithm on any iteration k . From the same line we see that the change of basis does not change λ , since the inner product of T_ψ with all the vectors \mathbf{v}_i on k -th iteration is basis invariant. This also means that the convergence of the algorithm, which is determined by λ (see line 4), is also not affected.

Algorithm 1 HOPM algorithm for estimating RTA of T_ψ with absolute accuracy ϵ [24].

```

1: procedure HOPM( $T_\psi, \epsilon$ )
2:   Let  $(\mathbf{v}_1^{(0)}, \dots, \mathbf{v}_n^{(0)})$ ,  $\lambda^{(0)}$  be a tuple of some  $n$  one-qubit state vectors and the
   corresponding entanglement eigenvalue.
3:   Initialise  $k$  to 1.
4:   while  $|\lambda^{(k)} - \lambda^{(k-1)}| > \epsilon$  do
5:     for  $i \in 1, \dots, n$  do
6:        $\mathbf{u}_i^{(k)} = T_\psi \times_i (\mathbf{v}_1^{(k)*}, \dots, \mathbf{v}_{i-1}^{(k)*}, \mathbf{v}_{i+1}^{(k-1)*}, \dots, \mathbf{v}_n^{(k-1)*})$ 
7:        $\mathbf{v}_i^{(k)} = \mathbf{u}_i^{(k)} / \|\mathbf{u}_i^{(k)}\|$ 
8:        $\lambda^{(k)} = |T_\psi \times (\mathbf{v}_1^{(k)*}, \dots, \mathbf{v}_n^{(k)*})|$ 
9:     increment  $k$ 
   return  $\lambda^{(k)}$  and  $(\mathbf{v}_1^{(k)}, \dots, \mathbf{v}_n^{(k)})$ 

```

2.2 Quantum implementation of HOPM for estimating the entanglement eigenvalue

In this section, we present an iterative quantum algorithm (Algorithm 2), which is a HOPM approach for approximating RTA with its crucial steps (lines 6-8 in Algorithm 1) performed on a quantum device. We will refer to this algorithm as QHOPM. The input for the algorithm is an n -qubit unitary operator $U_\psi \in \text{U}(2^n)$ that prepares the target state $|\psi\rangle = U_\psi |\mathbf{0}\rangle \in \mathbb{H}^n$, where $|\mathbf{0}\rangle = |0\rangle^{\otimes n}$ is the initial state of the system. The separable state $|\phi\rangle \in S_n$ is encoded as a tensor product of one-qubit x and z rotations acting on $|\mathbf{0}\rangle$:

$$|\phi\rangle = \bigotimes_{i=1}^n |\mathbf{v}_i\rangle = \bigotimes_{i=1}^n R_z(\varphi_i) R_x(\vartheta_i) |\mathbf{0}\rangle, \quad (5)$$

where $|\mathbf{v}_i\rangle$ are one-qubit states, and $\vartheta_i \in [0, \pi)$, $\varphi_i \in [0, 2\pi)$ are the angles used to encode $|\phi\rangle$. This choice of encoding of $|\mathbf{v}_i\rangle$ differs from any other encoding only by global phase and therefore is valid due to Remark 3. We choose an initial separable state $|\phi^{(0)}\rangle$ by randomly choosing the angles $(\vartheta_i^{(0)}, \varphi_i^{(0)})$ as a starting point for the approximation.

The first key steps of Algorithm 1 are lines 6 and 7 (consisting of the n -mode product and normalization) which yield an updated version of $|\mathbf{v}_i\rangle$.

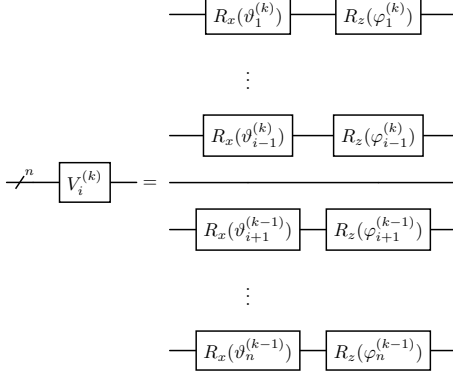


Fig. 1: Circuit representation of a separable state used for the i th mode update. The sub-circuit implements $V_i^{(k)}$ (see Eq. (8)), the vector part of the n -mode vector product for line 6 of Algorithm 1.

Proposition 4. Lines 6 and 7 of Algorithm 1 for the state $|\psi\rangle = U_\psi |\mathbf{0}\rangle$ at any iteration $k > 0$ are equivalent, up to a global phase, to the following update of $|\mathbf{v}_i^{(k)}\rangle$:

$$|\mathbf{v}_i^{(k)}\rangle = \sum_b v_{i,b}^{(k)} |b\rangle = \frac{\sum_b u_{i,b}^{(k)} |b\rangle}{\sqrt{\sum_b |u_{i,b}^{(k)}|^2}}, \quad (6)$$

where

$$u_{i,b}^{(k)} = \langle b_{[i]} | V_i^{(k)\dagger} U_\psi |\mathbf{0}\rangle, \quad |b_{[i]}\rangle = (|0\rangle^{\otimes(n-i)} \otimes |b\rangle \otimes |0\rangle^{\otimes(i-1)}) \quad (7)$$

is the b -th component of the n -mode vector product in line 6 having

$$V_i^{(k)} = \left[\bigotimes_{l=i+1}^n R_z(\varphi_l^{(k)}) R_x(\vartheta_l^{(k)}) \right] \otimes I \otimes \left[\bigotimes_{l=1}^{i-1} R_z(\varphi_l^{(k-1)}) R_x(\vartheta_l^{(k-1)}) \right], \quad (8)$$

(see Fig. 1), and $|b\rangle$ is a one-qubit computational basis.

Proof. We start with line 6 Algorithm 1 where we calculate the updated $\mathbf{u}_i^{(k)}$, the b -th component of which is

$$u_{i,b}^{(k)} = T_\psi \times \left(\mathbf{v}_1^{(k)*}, \dots, \mathbf{v}_{i-1}^{(k)*}, \mathbf{e}_b^*, \mathbf{v}_{i+1}^{(k-1)*}, \dots, \mathbf{v}_n^{(k-1)*} \right),$$

where \mathbf{e}_b is a one-qubit basis vector for the b -th component. Let us substitute to the right-hand side the following expressions for the components of T_ψ and $\mathbf{v}_{m \neq i}^{(t)}$ in terms

of U_ψ and $R_z R_x$:

$$\psi_{l_1, \dots, l_n} = \langle l_1 \dots l_n | U_\psi | \mathbf{0} \rangle; \quad v_{m,l}^{(t)} = \langle l | R_z(\varphi_m^{(t)}) R_x(\vartheta_m^{(t)}) | 0 \rangle,$$

and taking into account that the l -th component of \mathbf{e}_b in bra-ket notation is $\langle l | b \rangle$, we get for the b -th component of $\mathbf{u}_i^{(k)}$

$$\begin{aligned} u_{i,b}^{(k)} &= \sum_{l_1, \dots, l_n} \langle 0 | R_x^\dagger(\vartheta_1^{(k)}) R_z^\dagger(\varphi_1^{(k)}) | l_1 \rangle \dots \langle b | l_i \rangle \dots \\ &\quad \langle 0 | R_x^\dagger(\vartheta_n^{(k-1)}) R_z^\dagger(\varphi_n^{(k-1)}) | l_n \rangle \langle l_1 \dots l_n | U_\psi | 0 \rangle \\ &= \langle b_{[i]} | V_i^{(k)\dagger} U_\psi | \mathbf{0} \rangle, \end{aligned}$$

where $V_i^{(k)}$ is defined by Eq. (8). This expression corresponds to Eq. (7).

To prove that Eq. (7) yields line 6 of Algorithm 1 we perform the above steps in reverse, taking into account Remark 3.

Note, that for the components defined by (7) to correspond to a proper quantum state, they need to be normalized:

$$|\mathbf{v}_i^{(k)}\rangle = \frac{\sum_b u_{i,b}^{(k)} |b\rangle}{\sqrt{\sum_b |u_{i,b}^{(k)}|^2}},$$

which corresponds to the line 7 of Algorithm 1. \square

Proposition 4 allows us to understand which type of operations and measurements we should perform to implement lines 6 and 7 of the algorithm, in particular, we need to be able to obtain the updated pair of angles $(\vartheta_i^{(k)}, \varphi_i^{(k)})$ for further encoding the updated $|\mathbf{v}_i^{(k)}\rangle = R_z(\varphi_i^{(k)}) R_x(\vartheta_i^{(k)}) |0\rangle$.

2.2.1 Recovering one-qubit states with tomography

To obtain the angles $(\vartheta_i^{(k)}, \varphi_i^{(k)})$ for the one-qubit state $|\mathbf{v}_i^{(k)}\rangle$ of the i -th qubit at an arbitrary iteration k of QHOPM, we use the following one-qubit tomography procedure. Let $\mathcal{T}_i: \text{U}(2^n) \rightarrow [0, \pi) \times [0, 2\pi)$, which for some W returns the angles (ϑ_i, φ_i) , such that for $|w\rangle = W | \mathbf{0} \rangle$, $|q_i\rangle = R_z(\varphi_i) R_x(\vartheta_i) |0\rangle$ and any one-qubit basis state $|s\rangle$:

$$\langle s | q_i \rangle = \frac{\langle s_{[i]} | w \rangle}{\sqrt{|\langle s_{[i]} | w \rangle|^2 + |\langle s_{[i]}^\perp | w \rangle|^2}}, \quad (9)$$

and $|s_{[i]}^\perp\rangle$ is an orthogonal state to $|s_{[i]}\rangle$ defined in Eq. (7).

In our implementation, \mathcal{T}_i solves (using a classical device) the following system of equations

$$\begin{aligned}\langle Z \rangle_i &= 1 - 2P_i(0, W) = -\cos \vartheta_i; \\ \langle X \rangle_i &= 1 - 2P_i(+, W) = \sin \vartheta_i \sin \varphi_i; \\ \langle Y \rangle_i &= 1 - 2P_i(-i, W) = -\sin \vartheta_i \cos \varphi_i,\end{aligned}\tag{10}$$

where $\langle A \rangle_i = \langle q_i | A | q_i \rangle$; for the quantum system prepared in the state $|w\rangle$,

$$P_i(b, W) = |\langle b | q_i \rangle|^2 = \frac{|\langle b_{[i]} | w \rangle|^2}{|\langle b_{[i]} | w \rangle|^2 + |\langle b_{[i]}^\perp | w \rangle|^2}\tag{11}$$

is a probability of the i -th qubit being in the state $|b\rangle$, whilst other qubits are in the state $|0\rangle$. The probabilities $P_i(b, W)$ are obtained by querying the quantum system.

One way to obtain $P_i(b, W)$ is by direct measurement of $|\langle b_{[i]} | w \rangle|^2$, however the number of shots for a given accuracy in this approach grows exponentially with the number of qubits. In our implementation, we use a Hadamard test-based [41] procedure where the number of shots depends only on the accuracy and not the number of qubits.

First, we classically reconstruct the coefficients $C_s = \langle s | q_i \rangle$ (defined by Eq. (9)) for the state

$$|q_i\rangle = C_b |b\rangle + C_{b^\perp} |b^\perp\rangle$$

in some basis $B_b = \{|b\rangle, |b^\perp\rangle\}$. For this we measure the real and imaginary parts of $\langle s_{[i]} | w \rangle$ for each basis state $|s\rangle \in B_b$, using the Hadamard test procedure as follows.

1. Introduce an ancilla qubit, initialised in the state $|+\rangle$. The other qubits (referred to as data qubits in what follows) are initialised in the ground state $|\mathbf{0}\rangle$.
2. Perform a unitary operation W on the data qubits, controlled by the ancilla qubit.
3. Perform a unitary operation U_s^\dagger , that transforms $\langle 0 |$ to $\langle s |$ state, on the i -th data qubit, controlled by the ancilla qubit.
4. Measure $x_a = \langle X_a \rangle$ and $y_a = \langle Y_a \rangle$ on the ancilla qubit ($A_a = A \otimes I^n$).
5. Calculate $\langle s_{[i]} | w \rangle = x_a + iy_a$ (i is an imaginary unit).

In the case of QHOPM, $W = V_i^{(k)\dagger} U_\psi$ and $|q_i\rangle = |\mathbf{v}_i^{(k)}\rangle$ as defined in Eq. (6).

2.2.2 Measuring Entanglement

At the end of each iteration k , we need to measure $\lambda^{(k)}$.

Remark 5. *Line 8 of Algorithm 1 for a target state $|\psi\rangle = U_\psi |\mathbf{0}\rangle$ at any $k > 0$ iteration is equivalent to:*

$$\lambda^{(k)} = |\langle \mathbf{0} | V^{(k)\dagger} U_\psi |\mathbf{0}\rangle|,\tag{12}$$

where

$$V^{(k)} = \bigotimes_{i=1}^n R_z(\varphi_i^{(k)}) R_x(\vartheta_i^{(k)}).\tag{13}$$

Indeed, using the same procedure as in Proposition 4 we find:

$$\lambda^{(k)} = |\langle \mathbf{0} | V^{(k)\dagger} U_\psi |\mathbf{0}\rangle|.$$

From this Remark we see that $\lambda^{(k)}$ can be obtained by performing the Hadamard test-based measurement procedure as described in the previous Subsection with $W = V^{(k)\dagger}U_\psi$ (see Fig. 2(b)). We will denote this operation as

$$\Lambda: \mathbb{H}^n \rightarrow [0, 1]$$

$$|w\rangle \mapsto \lambda.$$

By combining the classical Algorithm 1 with the quantum operations above and making use of one-qubit tomography we execute the most memory-intensive operations (contractions of a tensor of size 2^n) of Algorithm 1 in the quantum domain using n qubits; these steps are given in Algorithm 2. The main steps of the algorithm implementation (lines 6 and 8 in Algorithm 2) are summarized in Fig. 2. The result is summarised in Theorem 6.

Algorithm 2 Iterative quantum implementation of Algorithm 1.

```

1: procedure QHOPM( $U_\psi, \epsilon$ )
2:   Choose  $(\vartheta_i^{(0)}, \varphi_i^{(0)}) \in [0, \pi) \times [0, 2\pi)$  for  $i = 1, \dots, n$ 
3:   initialise  $k$  to 0
4:   while  $|\lambda_n^{(k+1)} - \lambda_n^{(k)}| > \epsilon$  do
5:     for  $i \in 1, \dots, n$  do
6:        $\varphi_i^{(k+1)}, \vartheta_i^{(k+1)} = \mathcal{T}_i(V_i^{(k+1)\dagger}U_\psi |0\rangle)$ 
7:        $\lambda^{(k+1)} = \Lambda(V^{(k+1)\dagger}U_\psi |0\rangle)$ 
8:     increment  $k$ 
   return  $\lambda^{(k+1)}$  and  $\{(\vartheta_i^{(k+1)}, \varphi_i^{(k+1)})\}_{i=1\dots n}$ 

```

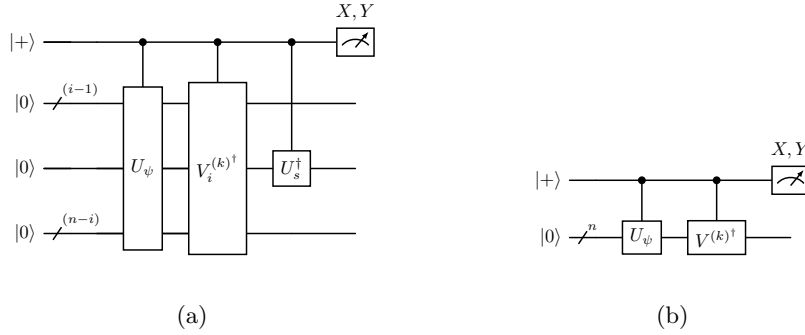


Fig. 2: Circuit representations of the main steps of QHOPM for the k -th iteration. (a) one-qubit tomography for measuring $u_{i,s}^{(k)}$ (see Sec. 2.2.1); (b) measuring $\lambda^{(k)}$. The meter labels show the operators to measure.

Theorem 6. *Given a unitary operator $U_\psi \in \text{U}(2^n)$, that prepares a target state $|\psi\rangle = U_\psi |\mathbf{0}\rangle$ and a sufficiently small ϵ , QHOPM (Algorithm 2) returns a pair λ and $\{(\vartheta_i, \varphi_i)\}_{i=1\dots n}$. Here $\{(\vartheta_i, \varphi_i)\}_{i=1\dots n}$ are the parameters of the encoding of a separable state $|\phi\rangle$. These values obey the following conditions:*

1. $|\phi\rangle$ is a rank-1 tensor approximation of $|\psi\rangle$.
2. $\lambda = |\langle\phi|\psi\rangle|$ is an approximation of the entanglement eigenvalue of $|\psi\rangle$.

Proof. First, we note that HOPM (Algorithm 1) satisfies points 1 and 2 of the theorem for the components T_ψ of the state $|\psi\rangle$ and one-qubit components \mathbf{v}_i of $|\phi\rangle$. Thus, to prove the points 1 and 2 for QHOPM it is enough to prove the equivalence of lines 6-8 of Algorithm 1 to lines 6 and 7 of Algorithm 2.

First, let us prove the equivalence of lines 6 and 7 of HOPM to line 6 of QHOPM. Having the encoding of the state $|\mathbf{v}_i^{(k+1)}\rangle$ in terms of the angles $(\vartheta_i^{(k+1)}, \varphi_i^{(k+1)})$, obtained in line 6 of QHOPM, we reconstruct the result of lines 6 and 7 of HOPM up to a global phase as follows, due to Proposition 4, Eq. (5) and Remark 3:

$$v_{i,b}^{(k+1)} = \langle b | \mathbf{v}_i^{(k+1)} \rangle = \langle b | R_z(\varphi_i^{(k+1)}) R_x(\vartheta_i^{(k+1)}) |0\rangle. \quad (14)$$

To show the other direction, having the components $v_{i,b}^{(k+1)}$, obtained in lines 6 and 7 of HOPM, we solve the system of equations Eq. (10) and recover the angles $(\vartheta_i^{(k+1)}, \varphi_i^{(k+1)})$. This proves the equivalence of lines 6-7 of HOPM to line 6 of QHOPM. This result does not depend upon i or k , thus, it is valid for any i and k .

In Remark 5 we showed how to use the obtained angles $(\vartheta_i^{(k+1)}, \varphi_i^{(k+1)})$ to calculate $\lambda^{(k+1)}$, which is just a way to rewrite line 8 of HOPM using U_ψ and $V^{(k+1)}$. The measurement of $\lambda^{(k+1)}$ is denoted as $\Lambda(V^{(k+1)\dagger} U_\psi |\mathbf{0}\rangle)$, which is line 7 of QHOPM. This shows the equivalence of line 8 of HOPM to line 7 of QHOPM for any $k > 0$ and finishes the proof. \square

2.2.3 Algorithm Complexity

Recall that n is the number of qubits in the input unitary U_ψ ¹ that defines the target state $|\psi\rangle$. Assuming the use of the Hadamard test for the n -qubit target state $|\psi\rangle$, QHOPM requires $n + 1$ qubits.

Each application of the tomography step on line 6 of Algorithm 2 requires 4 measurements to recover $|\mathbf{v}_i^{(k)}\rangle$, and each estimation of the scalar product at line 7 of Algorithm 2 requires 2 measurements. Thus, each iteration of the loop in line 4 uses $4n + 2$ measurements. Each measurement (assuming the Hadamard test) requires $\mathcal{O}(\epsilon^{-2})$ single-shot readouts² due to the Chernoff bound for absolute error ϵ . The total shot complexity of each iteration is $\mathcal{O}(n\epsilon^{-2})$.

The depth of the circuit used for measurements is defined by the depth of the circuit for U_ψ plus a constant. The constant is the sum of the depth of the separable state encoding ($V_i^{(k)}$ or $V^{(k)}$) and the overhead caused by the Hadamard test.

¹One may assume the circuit description of U_ψ is of length polynomial in n .

²Note it is possible to reduce the amount of measurements required to $\mathcal{O}(\epsilon^{-1})$ via amplitude amplification techniques.

QHOPM is a direct quantum implementation of the classical HOPM algorithm and so has the same convergence properties in the complex domain [26, 29]. While it is known that HOPM converges with complex tensors, however, the *rate* of convergence has only been shown (to our knowledge) for real tensors [42, 43, 44].

2.3 Simulation Results

In this section, we simulate our algorithm to evaluate its robustness to noise using the IBM Qiskit [45] platform (see Methods section for simulation details). We also show how to mitigate the effects of noise on the algorithm. We refer to target states by the notation State[n] for n qubits, for example GHZ[9] is the GHZ state with 9 qubits and Random[3] is a particular random state with 3 qubits.

When using HOPM we choose the minimum E_G from a sample of initial separable states, however (due to the finite number of shots) QHOPM tends to oscillate above and below the convergence value. We find the median gives a more accurate summary of the convergence value of QHOPM than the mean, perhaps reflecting some skew in the distribution.

For a given target state let \mathcal{F}_k represent a set of estimations of E_G for a sample of initial separable states at iteration $0 \leq k \leq K$. Let \bar{E}_G represent the value converged to by QHOPM, computed as the median of the values in $\mathcal{F} = \{\text{m}(\mathcal{F}_k) \mid k \in [K-5, \dots, K]\}$, where $\text{m}(\mathcal{A})$ is the median of the values in the set \mathcal{A} . Let $\text{IQR}_{\bar{E}_G}$ be the interquartile range for \mathcal{F} . We note that the choice of 5 final iterations here is arbitrary (statistically better results are obtained if one uses more iterations). Here we choose the median instead of the mean to avoid possible outliers induced by certain initial separable states.

We begin by verifying that our quantum implementation matches the classical algorithm and demonstrate the effect on convergence of the depolarising noise (DN) model (see Methods) with noise rate $p = 0.01$. We use the GHZ[9] state, which has a known $\hat{E}_G = 0.50$, as an example. In Fig. 3 we see a good correspondence with classical HOPM for 1×10^7 shots per measurement (yielding an expected error of $\epsilon \approx 3.2 \times 10^{-4}$ according to the Chernoff bound), that is QHOPM converges to the same value ($\bar{E}_G \approx 0.50$, $\text{IQR}_{\bar{E}_G} \lesssim 10^{-4}$) as classical HOPM ($\bar{E}_G = \hat{E}_G = 0.50$). Then we reduced the number of shots to 1×10^5 ($\epsilon \approx 3.2 \times 10^{-3}$) and we see convergence to $\bar{E}_G \approx 0.503$, within the slightly higher $\text{IQR}_{\bar{E}_G} \approx 0.005$ of the true value. These results are consistent with the Chernoff bound discussed in the previous Section. Finally, we introduced depolarising noise (DN) (see Methods) with error rate $p = 0.01$. Remarkably, the quantum algorithm still managed to converge with little variability ($\text{IQR}_{\bar{E}_G} \approx 0.003$), however, the value it converged to ($\bar{E}_G \approx 0.679$) is greater than the true value.

Notice that the distribution of E_G values found after 1 iteration by QHOPM is different from that found by HOPM for the same initial separable states. By the second iteration, HOPM and QHOPM converge to the same values. This divergence (from our experience) is normally not so noticeable, but of all the states we have studied (see Methods for the list of studied states), this effect is most pronounced in GHZ[9]. We assume that resolution errors, due to the reduced number of shots in the measurements, are amplified cumulatively for certain states (GHZ[9], in particular) during one-qubit tomography resulting in a different (but still improved) separable

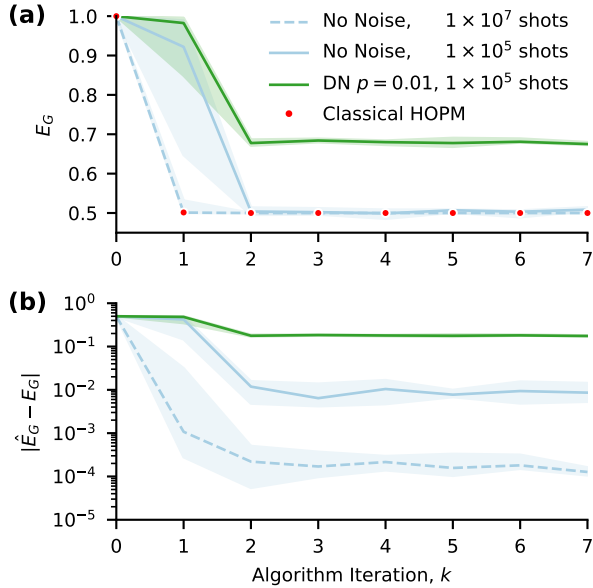


Fig. 3: The results of HOPM and QHOPM for (a) approximating the geometric entanglement E_G of GHZ[9] and (b) the absolute error ($|\hat{E}_G - E_G|$). The lines represent the median value for 10 random initial separable states for different numbers of shots per measurement and noise models (see legend). The shaded areas show the interquartile ranges.

state from what HOPM or QHOPM with infinite resolution would find. From this point on we proceed with 1×10^5 shots and the median over 10 initial separable states for all simulations (unless said otherwise) since it gives a sufficiently good convergence w.r.t. classical HOPM.

To evaluate the performance of QHOPM for random target states we ran QHOPM with no noise for 100 Random[n] target states each with 20 initial separable states with $n \in \{3, \dots, 6\}$ qubits. In Fig. 4 we summarize the results of the simulation. Here for each target state at iteration k we calculate the median result $m(\mathcal{F}_k)$ over 20 initial separable states and plot the median absolute difference $|\hat{E}_G - m(\mathcal{F}_k)|$ (and the interquartile range) over all the target states for each k and number of qubits n . We show that the median value of the absolute error $|\hat{E}_G - m(\mathcal{F}_k)|$ converges to the values less than 10^{-2} for any number of qubits, which is again consistent with the Chernoff bound. In the case of negligible noise, the accuracy of QHOPM depends only on the number of shots per measurement.

To explore the relationship between DN error rate p and the divergence of QHOPM's E_G value from HOPM's, we ran simulations with $p \in \{0.001, 0.01, 0.05\}$ representing “acceptable”, “bad” and “terrible” levels of noise, respectively. We used GHZ[9] and Random[6] as the target states. In Fig. 5(a) we see that for GHZ[9] when $p = 0.001$ QHOPM converges to $\bar{E}_G \approx 0.519$, $\text{IQR}_{\bar{E}_G} \approx 0.003$. The upper limit of error

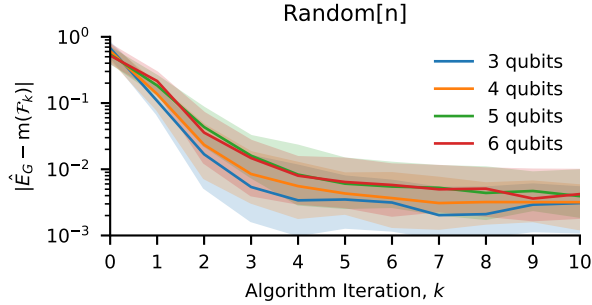


Fig. 4: The absolute error ($|\hat{E}_G - m(\mathcal{F}_k)|$) of QHOPM approximating E_G of Random[n] states with no noise. The lines represent the median absolute error over 100 Random[n] target states ($n \in \{3, \dots, 6\}$ qubits) between the best (minimal) HOPM results and the median results $m(\mathcal{F}_k)$ computed by QHOPM for each target state over 20 random initial separable states. The shaded areas show the interquartile ranges for the absolute error.

Table 1: Results of HOPM and QHOPM with different DN noise rates p for GHZ[9] and Random[6] states (see. Fig. 5). Minimum HOPM estimate for Random[6] is $E_G = 0.636$.

Target	DN p	Measured		Mitigated	
		\bar{E}_G	$\text{IQR}_{\bar{E}_G}$	\bar{E}'_G	$\text{IQR}_{\bar{E}'_G}$
GHZ[9]	0.001	0.519	0.003	0.499	0.003
	0.010	0.679	0.003	0.516	0.006
	0.050	0.946	0.002	0.554	0.019
Random[6]	0.001	0.657	0.003	0.638	0.003
	0.010	0.789	0.004	0.639	0.008
	0.050	0.978	0.000	0.661	0.029

rate p that is considered acceptable at this early stage of quantum computing is 0.01, at this level, the noise is causing our algorithm to converge to the value $\bar{E}_G \approx 0.679$ with $\text{IQR}_{\bar{E}_G} \approx 0.003$. At $p = 0.05$ the algorithm still converges with a similar variability but to the incorrect value $\bar{E}_G \approx 0.946$ with $\text{IQR}_{\bar{E}_G} \approx 0.002$. The results are also summarised in Table 1.

In Fig. 5(c) we give the results for the median E_G for Random[6]. With low noise ($p = 0.001$) QHOPM converges to $\bar{E}_G \approx 0.657$, $\text{IQR}_{\bar{E}_G} \approx 0.003$, which is within $\epsilon \approx 0.02$ w.r.t. the classical algorithm's result. Again, we see that as noise increases, the converged value increases: for $p = 0.01$ it goes to $\bar{E}_G \approx 0.789$ with $\text{IQR}_{\bar{E}_G} \approx 0.004$, and for $p = 0.05$ it goes to $\bar{E}_G \approx 0.978$ with $\text{IQR}_{\bar{E}_G} \approx 0.000$. We note that the interquartile range of the converged values is within our measurement tolerance $\epsilon \approx 0.003$ (defined by the chosen number of shots; see Methods).

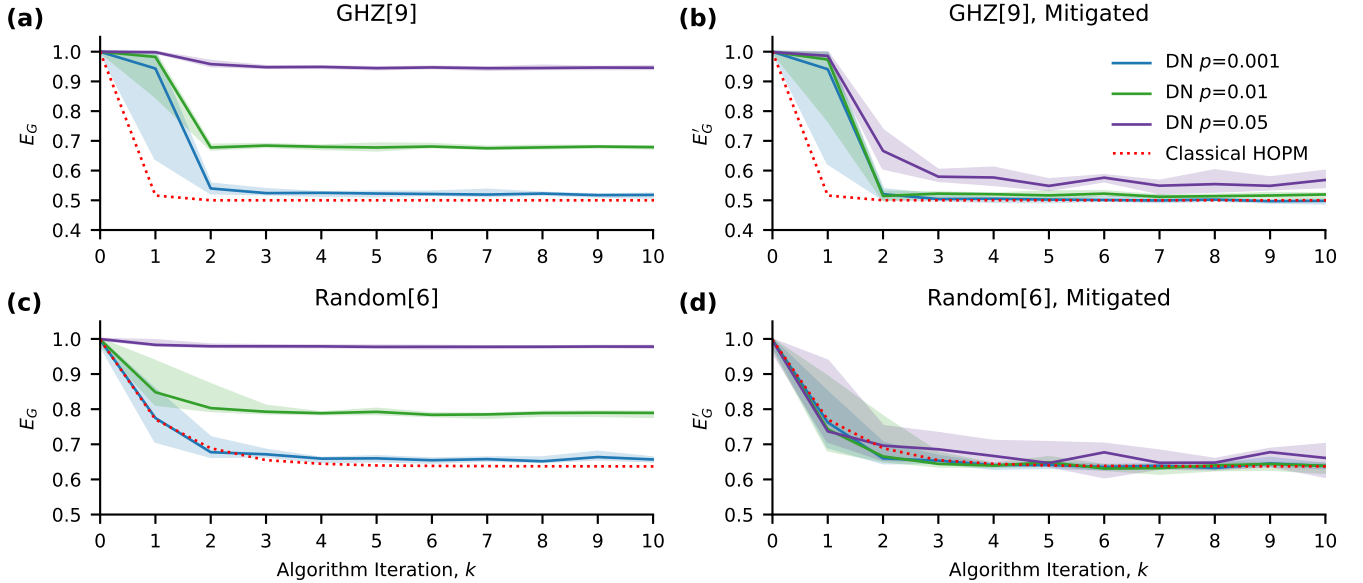


Fig. 5: Simulation results for QHOPM on target states GHZ[9] and Random[6] with the DN model and its mitigation. (a) and (c) show the simulation results for QHOPM with input target states GHZ[9] and Random[6], respectively, for different DN error rates; (b) and (d) show the results of our mitigation procedure (see Eq. (26)) applied to results in (a) and (c), respectively. Solid lines represent the median geometric entanglement, E_G , over the results for different initial separable states and the shaded colours represent the interquartile range. The colour of the lines represents the DN noise rate used for the simulation (see legend). Red dotted lines show the results of classical HOPM.

We see the same effects for: GHZ[3], GHZ[6] (Supplemental Figure 7(a),(c)); Random[3], Random[9] (Supplemental Figure 10(a),(e)); the well studied W[3] state with $\hat{E}_G = 5/9$ (Supplemental Figure 8(a)); and the important ring cluster states Ring[3], Ring[6], Ring[9], (Supplemental Figure 9(a),(c),(e)). We also observe that the shift, induced by noise, increases as the number of qubits increases.

We then characterised the shift in \bar{E}_G induced by the noise as a function of circuit depth and noise rate. The resulting model (see Methods), based on the simple assumption that the depolarising channel is applied with a constant error rate p after each of d layers of gates, yields a formula Eq. (26) that approximates the mitigated GE, E'_G , expected without noise. Similarly to \bar{E}_G we define \bar{E}'_G as the mitigated result of QHOPM, computed as the median of the values in $\mathcal{F}' = \{m(\mathcal{F}'_k) \mid k \in [K-5, \dots, K]\}$, where \mathcal{F}'_k represents a set of mitigated values E'_G for a sample of initial separable states at iteration $0 \leq k \leq K$. Similarly $\text{IQR}_{\bar{E}'_G}$ is the interquartile range of \mathcal{F}' . We

observe in Fig. 5(b) the effect of the mitigation on GHZ[9]. For $p = 0.001$, the mitigated value $\overline{E}'_G \approx 0.499$ with $\text{IQR}_{\overline{E}'_G} = 0.003$, which corresponds to the true value. However, for $p = 0.01$, $\overline{E}'_G \approx 0.516$ with $\text{IQR}_{\overline{E}'_G} = 0.006$ is the result. For $p = 0.05$ mitigation is still helpful and adjusts the noisy value to $\overline{E}'_G \approx 0.554$ ($\text{IQR}_{\overline{E}'_G} = 0.019$). We see in Fig. 5(d) that the mitigation for the state Random[6] gives better results: for $p = 0.001$ E_G being mitigated to $\overline{E}'_G \approx 0.638$ ($\text{IQR}_{\overline{E}'_G} = 0.003$), for $p = 0.01$ to $\overline{E}'_G \approx 0.639$ ($\text{IQR}_{\overline{E}'_G} = 0.008$), and for $p = 0.05$ to $\overline{E}'_G \approx 0.661$ ($\text{IQR}_{\overline{E}'_G} = 0.029$). We suspect that the observed improvement in mitigation is due to the increased gate density of the Random[6] circuit compared to GHZ[9]. Our model assumes the noise channel is applied to all qubits d times (for circuit depth d) with the same error rate p . However, the DN implementation in Qiskit applies the channel only when there is a gate applied to the qubit. The structure of the circuit for GHZ[9] is one of the worst cases for our mitigation method since it includes a chain of 8 CNOTs traversing the 9 qubits one by one, leading to a deep but sparse circuit structure.

We also applied our mitigation technique to other GHZ states (Supplemental Fig. 7(b),(d),(f)), the W state (Supplemental Figure 8(b)), some Cluster Ring states (Supplemental Figure 9(b),(d),(f)), and some Random states (Supplemental Figure 10(b),(d),(f)).

Finally, we apply our mitigation technique to results obtained with more realistic noise models. We consider the Qiskit “FakeLima” (representing an older 5 qubit device) and “FakeSherbrooke” (representing a newer device) Qiskit backends that are calibrated to match the error profile of physical devices. To apply our mitigation technique we need to estimate the noise rate p for DN that would approximate the quantum device’s noise. To do this we apply QHOPM to the GHZ state, where the true value \hat{E}_G is known. We then use the ratio between the measured \overline{E}_G and the true value \hat{E}_G to estimate p (see Methods, Eq. (27)).

Since GHZ[9] is calibrated against itself, to demonstrate our mitigation technique on realistic noise models we show only the state Random[6] (p estimated with GHZ[6]). The graph for GHZ[9] is in Supplemental Figure 7(f). In Fig. 6 we show the median absolute error of the QHOPM results for Random[6] state within (a) FakeSherbrooke and (c) FakeLima backends, and their mitigation results (b) and (d), respectively. See Supplementary Materials for more state simulations and mitigation results for these noise models.

3 Discussion

In this work we presented QHOPM, an iterative quantum algorithm for the approximation of the geometric measure of entanglement of pure states on near term quantum devices as well as a simple noise mitigation technique to improve its experimental resolution. QHOPM is the quantum adaptation of the well-known classical HOPM approach [20, 21, 22, 26, 27, 29] for rank-1 tensor approximation.

While QHOPM does not converge differently than classical HOPM and gives similar results (assuming a sufficient amount of shots and relatively low noise rate) its

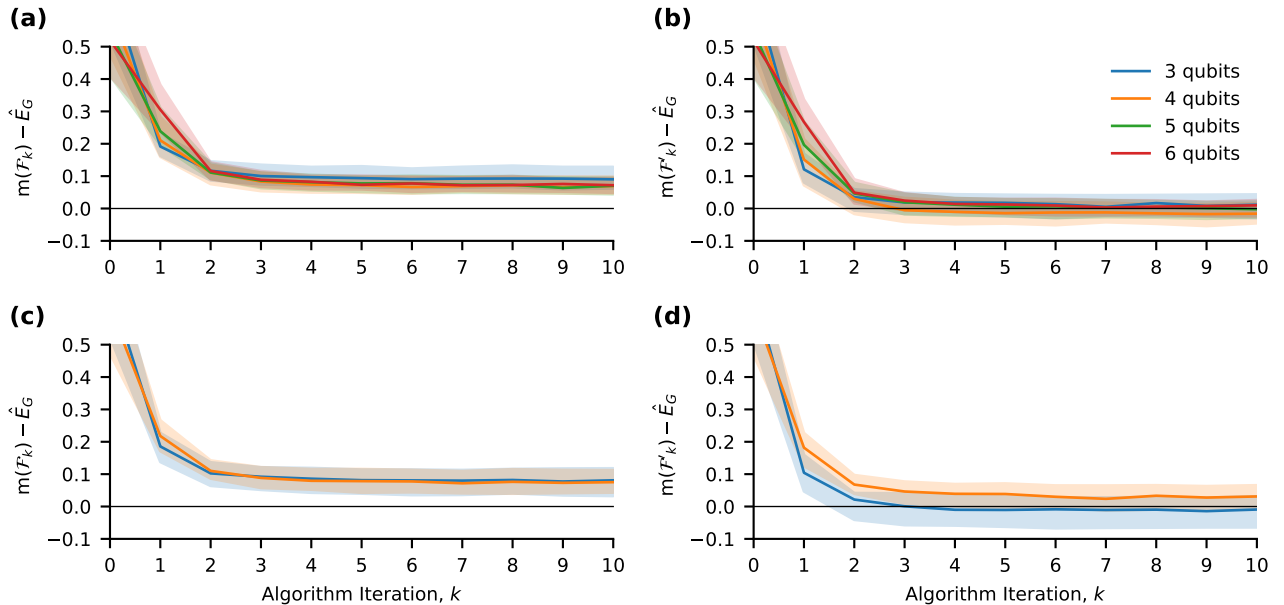


Fig. 6: The error $(m(\mathcal{F}_k) - \hat{E}_G)$ of QHOPM approximating E_G for 100 different samples of $\text{Random}[n]$ with realistic noise models and their mitigation. (a) and (b) show unmitigated and mitigated results, respectively, for $\text{Random}[n]$ with $n \in \{3, 4, 5, 6\}$, simulated with the FakeSherbrooke Qiskit backend. (c) and (d) show the same for the FakeLima Qiskit backend ($n \in \{3, 4\}$ since FakeLima imitates a 5 qubit device). Solid lines represent the median error over the initial separable states and the shaded colours represent the interquartile range. The colour of the lines represents the number of qubits (see legend).

potential utility lies in the observation that it requires only $n + 1$ qubits to compute the GE of a quantum state (on n qubits) while classical HOPM naively requires an exponential data structure (and so exponential runtime) to work with quantum states. We also show that the number of measurements required per algorithm iteration scales linearly with n . In our work, to avoid the problem of post-selection we have assumed Hadamard test-based measurements, which have recently been successfully implemented on real devices [46].

We observed that the effect of depolarising noise on QHOPM for the studied noise rates ($p \leq 0.05$) and number of shots (10^5) does not affect its convergence, but rather shifts the final result. The same observation was made in simulations using more realistic noise models implemented in IBM Qiskit’s FakeLima and FakeSherbrooke simulation backends. This allowed us to assume and successfully apply the mitigation technique developed for the DN model on these unknown noise channels. The noise rate for the unknown models was estimated using $\text{GHZ}[n]$ as a reference state with a known GE.

Another mitigation approach is presented in [47], where the authors assumed that the DN channel is applied only on the final stage before each measurement with the “total” error rate p_{tot} , which they propose to recover from measuring $\text{Tr}(\rho^2)$. This approach is equivalent to ours if we use $p_{tot} = 1 - q^d$ and treat p and d as parameters (see Remark 8).

We note that noise analysis was not the main topic of this work and the assumptions we made are simplified. A more consistent and rigorous approach would be to consider the application of the DN channel with different noise rates to individual gates twirled over the Haar distribution (using, say, Clifford 2-design) [48, 49] or to study the noise model of a particular quantum device.

To our knowledge, the only other quantum algorithms for calculating geometric entanglement are variational algorithms where the ansatz is a separable state [32, 31]. We now compare one of these, the VDGE algorithm [31], with QHOPM. VDGE converges more slowly than QHOPM, needing on the order of 10^2 iterations compared to QHOPM’s 10^0 , with noise or without. In a noiseless simulation (for Haar random target states) with 3 qubits, the median absolute error of VDGE’s best results for each target state converges to approximately 10^{-4} (see Fig. 3 in [31]). As the number of qubits increases to six, the error grows to approximately 10^{-2} . In similar simulations with noiseless QHOPM, the accuracy of the results seems less dependent on the number of qubits and more on the number of shots, satisfying the Chernoff bound (see Fig. 4). So in the noiseless case, while VDGE is more accurate with fewer shots per measurement on small numbers of qubits, QHOPM can improve its accuracy by increasing the number of shots, independent of the number of qubits (at least, for the range of qubits studied). When realistic noise is introduced, the accuracy of QHOPM’s results (see Fig. 6) are of the order of VDGE results (see Fig. 6 [31]). The authors of VDGE, use an optimizer (complex simultaneous perturbation stochastic approximation) that is claimed to be robust against noise. We note that, in the presence of noise, QHOPM still converges to a value and simple mitigation techniques recover a number closer to the noiseless value. Like QHOPM, these variational approaches are sensitive to the initial separable state and one is never sure if the result obtained is a local minimum or the global minimum. Also, like any quantum variational approach, VDGE is prone to have barren plateaus as the number of qubits grows, which makes it difficult for the algorithm to find a good solution. In all examples we have studied, QHOPM converges in approximately 4 iterations, however we have no formal statement about the convergence rate of the algorithm. The convergence rate of QHOPM will be a complex extension of the known HOPM convergence rate for real valued tensors [43, 44].

We observe that HOPM may be extended with a shift parameter to a so-called shifted HOPM [50, 27] or Gauss-Seidel method [29]. In the Supplementary Materials we show how we incorporate this change in our algorithm.

An interesting future direction is to extend our method to approximating geometric entanglement of mixed states [19]. For example, the authors of [22] presented a method for approximating GE of a mixed state based on the connection to the so-called revised GE [51] and Uhlmann’s theorem [52]. The classical implementation of the method given in [22] may be naively modified to incorporate techniques presented in the current

work for some intermediate steps, but the calculation will still be performed largely on the classical side. Further work is needed to effectively incorporate QHOPM with this method.

Finally, we observe that our algorithm is a quantum application of the alternating least squares (ALS) method applied to the particular system of non-linear equations for estimating rank-1 tensor approximation. The ALS method by itself is an area of interest in classical machine learning [53, 54], perhaps a variant of our approach would be of use in a suitable problem domain.

Methods

3.1 QHOPM simulation

We simulate the Hadamard test variant of QHOPM using the Qiskit [45] platform (IBM Qiskit Version 0.46.0). We find in practice that the algorithm gives sufficiently good results when each individual simulation uses 1×10^5 shots which corresponds to an absolute accuracy $\epsilon \approx 0.003$.

For a given a target state, regions of initial separable states will converge to different local minima [24]. When using the HOPM algorithm one might try many initial separable states and choose the minimum value obtained. In this work we use 10 random initial states to demonstrate the variation between initial starting points.

To investigate the effect of noise on our algorithm, we use the depolarising noise (DN) model [52] and more realistic noise models implemented in the “FakeLima” and “FakeSherbrooke” Qiskit backends, developed to mimic real IBM hardware. To simplify the analysis, we let the parameter of the DN model (referred to in this work as “noise rate” or “error rate”) $p \in \{0, 0.001, 0.01, 0.05\}$ and apply DN to all one-, two- and three-qubit gates used in our circuits via the Qiskit AerSimulator.

To demonstrate the performance of QHOPM we chose the following target states:

- 3 qubit W state, with known $E_G = 5/9$ [19];
- 3, 4, 5, 6, and 9 qubit GHZ states, each with known $E_G = 0.5$;
- 3, 6 and 9 qubit ring cluster states [3];
- 3, 4, 5, 6 and 9 qubit random states.

To generate Random[n] states we created quantum circuits with the following method: we sampled gates (uniformly at random) from the gate set of CNOT and Qiskit’s U gate (general single qubit rotation) with random angles and applied them to uniformly random selected qubits. This process was iterated until the circuit depth reached 10.

The initial random separable states $V^{(0)}$ (see Eq. (5)) were chosen by sampling uniformly at random $\vartheta_i \in [0, \pi)$ and $\varphi_i \in [0, 2\pi)$ for $i = 1, \dots, n$.

3.2 Depolarising noise mitigation

To mitigate the effects of noise on the simulation results we assume the depolarising noise (DN) model [52] in our simulations. The DN channel for a system of n qubits,

applied to all the qubits is defined as [52, 49]

$$\mathcal{E}(\rho) = (1 - p)\rho + p\frac{1}{2^n}I^n, \quad (15)$$

where I is a 2-dimensional identity matrix; $0 \leq p \leq 4^n/(4^n - 1)$ is a parameter of the model (which we will refer to as noise rate). When $p = 1$ the channel is fully depolarising. When $p = 4^n/(4^n - 1)$ the channel is equivalent to random Pauli errors applied (uniformly) on each qubit with equal probability.

A more consistent approach would be to “convert” the noise channel in the system to depolarising noise using, say, Clifford 2-design [48, 49] and assume different noise rates for different types of gates. As our work was not aimed at detailed noise analysis we consider the following simplification: we assume that the DN channel is applied d times at a constant rate p to *all qubits* after each layer of gates, where d is the circuit depth (maximum number of operations on a qubit in the circuit). The DN channel commutes with any unitary operation:

$$U \mathcal{E}(\rho) U^\dagger = U \left((1 - p)\rho + p\frac{I}{2^n} \right) U^\dagger = \mathcal{E}(U\rho U^\dagger),$$

which allows to apply the channel d times at the end of the circuit:

$$\begin{aligned} \rho = \mathcal{E}^d(\rho') &= (1 - p)^d \rho' + \frac{p}{2^n} \sum_{i=1}^d (1 - p)^{d-i} I \\ &= q^d \rho' + \frac{1 - q^d}{2^n} I, \end{aligned} \quad (16)$$

where $q = (1 - p)$; ρ' is a density matrix of a pure state with no noise. The number d is also be understood as the number of times that the DN channel affects the state with the error rate p .

Proposition 7. *Given the DN channel defined by Eq. (16), in terms of the Hadamard test procedure and sufficient number of shots, the measured $P_i(s)$ ($P_i(s, U)$ for some arbitrary U) and $\lambda^{(k)}$ can be expressed as*

$$P_i(s) = \frac{P'_i(s)}{1 - \eta P'_i(s^\perp)} \approx (1 + \eta P'_i(s^\perp) + \dots) P'_i(s); \quad (17)$$

$$\lambda^{(k)} = q^d \sqrt{1 - \eta \sin^2 \gamma'} \lambda'^{(k)}, \quad (18)$$

where $\eta = (1 - q^2) > 0$; $P'_i(s)$, $P'_i(s^\perp)$ and $\lambda'^{(k)}$ are the noise-free values of $P_i(s)$, $P_i(s^\perp)$ and $\lambda^{(k)}$, respectively; dots in Eq. (17) correspond to the terms of the second order and higher in η ; γ' is the phase of the noise-free scalar product $\langle \mathbf{0} | V^{(k)\dagger} U_\psi | \mathbf{0} \rangle = \lambda'^{(k)} e^{-i\gamma'}$, which is recovered from

$$\tan \gamma' = q \frac{\langle Y_a \rangle}{\langle X_a \rangle}. \quad (19)$$

Proof. To obtain $P_i(s)$, defined by Eq. (11), we need to measure $|\langle b_{[i]}|w\rangle|$, which in terms of the Hadamard test procedure is done by measuring

$$\begin{aligned}\langle X_a \rangle &= 1 - 2P^{(a)}(+), \\ \langle Y_a \rangle &= 1 - 2P^{(a)}(-i),\end{aligned}\tag{20}$$

where

$$\begin{aligned}P^{(a)}(+)&= \text{Tr}(|+\rangle\langle +| \otimes I^{n-1} \rho) = q^d P^{(a)'}(+)+\frac{1-q^d}{2}, \\ P^{(a)}(-i)&= \text{Tr}(S^\dagger |+\rangle\langle +| S \otimes I^{n-1} \rho) = q^{d+1} P^{(a)' }(-i)+\frac{1-q^{d+1}}{2}\end{aligned}\tag{21}$$

are the ‘‘noisy’’ probabilities of the ancilla qubit being in the state $|+\rangle$ and $|-i\rangle$, respectively, and $P^{(a)'}(+)$ and $P^{(a)' }(-i)$ are their ‘‘non-noisy’’ counterparts. After substituting Eq. (21) to Eq. (20), for $u_{i,s}^{(k)}$ we have:

$$|\langle b_{[i]}|w\rangle|^2 = \langle X_a \rangle^2 + \langle Y_a \rangle^2 = q^{2d}[1 - (1 - q^2) \sin^2 \gamma'] |\langle b_{[i]}|w\rangle'|^2,\tag{22}$$

where $\langle b_{[i]}|w\rangle'$ is a non-noisy value of $\langle b_{[i]}|w\rangle$; γ' is the phase of $\langle b_{[i]}|w\rangle' = e^{i\gamma'} |\langle b_{[i]}|w\rangle'|$, which originates from the global phase and local z -rotations. We know (see Remark 3) that in the absence of noise, the global phase does not affect the convergence of the algorithm, however since d for $\langle Y_a \rangle' = (\sin \gamma' |\langle b_{[i]}|w\rangle'|)$ is larger, in the noisy case we will have additional terms in the sum in Eq. (22). In the experiment γ' is recovered from

$$\tan \gamma' = \frac{\langle Y_a \rangle'}{\langle X_a \rangle'} = q \frac{\langle Y_a \rangle}{\langle X_a \rangle}.$$

Similarly, we get

$$|\langle b_{[i]}^\perp|w\rangle|^2 = q^{2d+2}[1 - (1 - q^2) \sin^2 \gamma'] |\langle b_{[i]}^\perp|w\rangle'|^2,\tag{23}$$

where the angle γ' is the same as for the state $|b\rangle$, since $U_{b^\perp} = U_b X$ does not change the phase³.

Substituting Eq. (22) and Eq. (23) to Eq. (11), we have for $P_i(s)$:

$$\begin{aligned}P_i(s) &= \frac{|\langle b_{[i]}|w\rangle'|^2}{|\langle b_{[i]}|w\rangle'|^2 + |\langle b_{[i]}^\perp|w\rangle'|^2 - \eta |\langle b_{[i]}^\perp|w\rangle'|^2} \\ &= \frac{P_i'(s)}{1 - \eta P_i'(s^\perp)} \approx (1 + \eta P_i'(s^\perp) + \dots) P_i'(s),\end{aligned}\tag{24}$$

³For real hardware or more realistic simulations, the phase might change depending upon the implementation of X , however, it will not change $P_i(s)$ drastically.

where $\eta = (1 - q^2) > 0$; the right-hand side is the Taylor expansion of the left side near $\eta = 0$; $P'_i(s^\perp)$ is a non-noisy value of $P_i(s^\perp)$. This proves the first statement of the Proposition.

Following the same steps for $\lambda^{(k)}$, assuming that the noise does not affect one-qubit tomography results, we have in terms of the Hadamard test procedure:

$$\lambda^{(k)2} = \langle X_a \rangle^2 + \langle Y_a \rangle^2 = q^{2d}[1 - \eta \sin^2 \gamma'] \lambda'^{(k)2}, \quad (25)$$

where γ' is the argument of non-noisy $\langle \mathbf{0} | V^{(k)\dagger} U_\psi | \mathbf{0} \rangle = e^{i\gamma'} \lambda'^{(k)}$ and is obtained using Eq. (19); $\lambda'^{(k)}$ is a non-noisy entanglement eigenvalue. This proves the second statement of the Proposition. \square

If all the η terms in Eq. (17) are negligible ($p \ll 1$), the one-qubit tomography procedure \mathcal{T}_i will return angles with errors of similar magnitude for any circuit depth. If these errors can be neglected, the convergence condition of QHOPM, given in line 4 in Algorithm 2, will change only by the prefactor defined in Eq. (18). In this work, the largest error rate that we have studied is $p = 0.05$ which gives $\eta \approx 0.1$. Thus, according to Proposition 7 and assuming $P'_i(s) = P'_i(s^\perp) = 0.5$, $P_i(s)$ changes at most by approximately 0.05. This change does not affect the convergence, as it is seen from the simulations. We neglect this effect in what follows and take into account only the changes of $\lambda^{(k)}$, which even for relatively shallow U_ψ may be significant. With these assumptions we approximate the true E'_G as follows:

$$E'_G = 1 - \frac{1 - E_G}{q^{2d}[1 - \eta \sin^2 \gamma']}, \quad (26)$$

where γ' is obtained from Eq. (19). The denominator of the lower bound $E'_G \geq 1 - \frac{1 - E_G}{q^{2d+2}}$ is always less (or equal) than one, which means that $E_G \geq E'_G$ within our assumptions, which corresponds to the observed simulation results.

Remark 8. Proposition 7 and Eq. (26) are valid for a DN channel with the noise rate $p_{tot} = 1 - q^d$ applied once in the end of the circuit just before the measurements.

This is evident from comparing Eq. (15) and Eq. (16), and allows us to conclude that the made simplified assumption, with the appropriate choice of parameters p and d , are valid for any noise channel that is approximated by DN model.

3.3 Mitigating error for arbitrary noise models

To mitigate the results of our algorithm on hardware or simulations where the noise model is usually unknown, we use the following procedure. We run the algorithm on a reference state with a known \hat{E}_G and measure the noisy value E_G . In our case we chose GHZ[n] with $\hat{E}_G = 0.50$ since the value is consistent for any number of qubits. Using this value and Eq. (26) we calculate p as follows:

$$p = 1 - \left(\frac{1 - \hat{E}_G}{1 - E_G} \right)^{2d}. \quad (27)$$

The mitigation procedure now proceeds as outlined in the depolarising noise case.

Acknowledgements

Equal1 was funded by DTIF: QCoIr (Enterprise Ireland Project Number: 166669/RR), and EIC project QUENML Quantum-enhanced Machine Learning, 190105118. Simone Patscheider was partly funded by the University of Trento Masters program. Alessandra Bernardi was partially funded by GNSAGA of INDAM, TensorDec Laboratory and by the European Union under NextGenerationEU. PRIN 2022 Prot. n. 2022ZRRL4C_004. We also thank Nikolaos Petropoulos for useful discussions.

References

- [1] Horodecki, R., Horodecki, P., Horodecki, M. & Horodecki, K. Quantum entanglement. *Rev. Mod. Phys.* **81**, 1–94 (2009). URL <http://arxiv.org/abs/quant-ph/0702225>.
- [2] Wootters, W. K. Quantum entanglement as a quantifiable resource. *Philos. Trans. R. Soc. A* **356**, 1717–1731 (1998). URL <https://royalsocietypublishing.org/doi/10.1098/rsta.1998.0244>.
- [3] Gühne, O. & Tóth, G. Entanglement detection. *Phys. Rep.* **474**, 1–75 (2009). URL <https://www.sciencedirect.com/science/article/pii/S0370157309000623>.
- [4] Broadbent, A. & Schaffner, C. Quantum Cryptography Beyond Quantum Key Distribution. *Des. Codes Cryptogr.* **78**, 351–382 (2016). URL <http://arxiv.org/abs/1510.06120>.
- [5] Vidal, G. Efficient classical simulation of slightly entangled quantum computations. *Phys. Rev. Lett.* **91**, 147902 (2003). URL <http://arxiv.org/abs/quant-ph/0301063>. ArXiv:quant-ph/0301063.
- [6] Gottesman, D. Theory of fault-tolerant quantum computation. *Phys. Rev. A* **57**, 127–137 (1998). URL <https://link.aps.org/doi/10.1103/PhysRevA.57.127>.
- [7] Gottesman, D. The Heisenberg Representation of Quantum Computers. *Group22: Proceedings of the XXII International Colloquium on Group Theoretical Methods in Physics* (1998). URL <http://arxiv.org/abs/quant-ph/9807006>.
- [8] Aaronson, S. & Gottesman, D. Improved simulation of stabilizer circuits. *Phys. Rev. A* **70**, 052328 (2004). URL <https://link.aps.org/doi/10.1103/PhysRevA.70.052328>.
- [9] Gross, D., Flammia, S. T. & Eisert, J. Most quantum states are too entangled to be useful as computational resources. *Phys. Rev. Lett.* **102**, 190501 (2009). URL <https://link.aps.org/doi/10.1103/PhysRevLett.102.190501>.
- [10] Patti, T. L., Najafi, K., Gao, X. & Yelin, S. F. Entanglement devised barren plateau mitigation. *Phys. Rev. Research* **3**, 1–10 (2021). URL <https://link.aps.org/doi/10.1103/PhysRevResearch.3.033090>.
- [11] Marrero, C. O., Kieferová, M. & Wiebe, N. Entanglement Induced Barren Plateaus. *PRX Quantum* **2**, 1–14 (2021). URL <http://arxiv.org/abs/2010.15968>.
- [12] Georgiev, D. D. & Gudder, S. P. Sensitivity of entanglement measures in bipartite pure quantum states. *Mod. Phys. Lett. B* **36**, 1–26 (2022).

- [13] Wootters, W. K. Entanglement of formation of an arbitrary state of two qubits. *Phys. Rev. Lett.* **80**, 2245–2248 (1998). URL <https://link.aps.org/doi/10.1103/PhysRevLett.80.2245>.
- [14] Love, P. J. *et al.* A Characterization of Global Entanglement. *Quantum Inf. Process.* **6**, 187–195 (2007). URL <https://doi.org/10.1007/s11128-007-0052-7>.
- [15] Plenio, M. B. & Virmani, S. An introduction to entanglement measures. *Quantum Info. Comput.* **7**, 1–51 (2007).
- [16] Dür, W., Vidal, G. & Cirac, J. I. Three qubits can be entangled in two inequivalent ways. *Phys. Rev. A* **62**, 1–11 (2000). URL <https://link.aps.org/doi/10.1103/PhysRevA.62.062314>.
- [17] Shimony, A. Degree of Entanglement. *Ann. N.Y. Acad. Sci.* **755**, 675–679 (1995). URL <https://onlinelibrary.wiley.com/doi/abs/10.1111/j.1749-6632.1995.tb39008.x>.
- [18] Barnum, H. & Linden, N. Monotones and invariants for multi-particle quantum states. *J. Phys. A: Math. Gen.* **34**, 1–12 (2001). URL <https://dx.doi.org/10.1088/0305-4470/34/35/305>.
- [19] Wei, T.-C. & Goldbart, P. M. Geometric measure of entanglement and applications to bipartite and multipartite quantum states. *Phys. Rev. A* **68**, 1–12 (2003). URL <https://link.aps.org/doi/10.1103/PhysRevA.68.042307>.
- [20] Shimoni, Y., Shapira, D. & Biham, O. Entangled quantum states generated by Shor’s factoring algorithm. *Phys. Rev. A* **72**, 062308 (2005). URL <https://link.aps.org/doi/10.1103/PhysRevA.72.062308>.
- [21] Most, Y., Shimoni, Y. & Biham, O. Entanglement of periodic states, the quantum fourier transform, and shor’s factoring algorithm. *Phys. Rev. A* **81**, 052306 (2010). URL <https://link.aps.org/doi/10.1103/PhysRevA.81.052306>.
- [22] Streltsov, A., Kampermann, H. & Bruß, D. Simple algorithm for computing the geometric measure of entanglement. *Phys. Rev. A* **84**, 022323 (2011). URL <https://link.aps.org/doi/10.1103/PhysRevA.84.022323>.
- [23] Teng, P. Accurate calculation of the geometric measure of entanglement for multipartite quantum states. *Quantum Inf. Process.* **16**, 1–17 (2017). URL <http://arxiv.org/abs/1609.02076>.
- [24] De Lathauwer, L., De Moor, B. & Vandewalle, J. On the best rank-1 and rank- (r_1, r_2, \dots, r_n) approximation of higher-order tensors. *SIAM J. Matrix Anal. Appl.* **21**, 1324–1342 (2000). URL <https://doi.org/10.1137/S0895479898346995>.
- [25] Hayashi, M., Markham, D., Murao, M., Owari, M. & Virmani, S. The geometric measure of entanglement for a symmetric pure state with non-negative amplitudes. *J. Math. Phys.* **50**, 122104 (2009). URL <https://doi.org/10.1063/1.3271041>.
- [26] Ni, G., Qi, L. & Bai, M. Geometric Measure of Entanglement and U-Eigenvalues of Tensors. *SIAM J. Matrix Anal. Appl.* **35**, 73–87 (2014). URL <https://epubs.siam.org/doi/abs/10.1137/120892891>.
- [27] Hu, S., Qi, L. & Zhang, G. Computing the geometric measure of entanglement of multipartite pure states by means of non-negative tensors. *Phys. Rev. A* **93**, 012304 (2016). URL <https://link.aps.org/doi/10.1103/PhysRevA.93.012304>.
- [28] Qi, L., Zhang, G. & Ni, G. How entangled can a multi-party system possibly

- be? *Phys. Lett. A* **382**, 1465–1471 (2018). URL <https://www.sciencedirect.com/science/article/pii/S0375960118303621>.
- [29] Zhang, M., Ni, G. & Zhang, G. Iterative methods for computing U-eigenvalues of non-symmetric complex tensors with application in quantum entanglement. *Comput. Optim. Appl.* **75**, 779–798 (2020). URL <https://doi.org/10.1007/s10589-019-00126-5>.
- [30] Chatelin, F. *Eigenvalues of Matrices* (Society for Industrial and Applied Mathematics, 2012).
- [31] Muñoz Moller, A., Pereira, L., Zambrano, L., Cortés-Vega, J. & Delgado, A. Variational determination of multiqubit geometrical entanglement in noisy intermediate-scale quantum computers. *Phys. Rev. Applied* **18**, 1–7 (2022). URL <https://link.aps.org/doi/10.1103/PhysRevApplied.18.024048>.
- [32] Consiglio, M., Apollaro, T. J. G. & Wieśniak, M. Variational approach to the quantum separability problem. *Phys. Rev. A* **106**, 1–12 (2022). URL <https://link.aps.org/doi/10.1103/PhysRevA.106.062413>.
- [33] Bernardi, A., Carlini, E., Catalisano, M. V., Gimigliano, A. & Oneto, A. The hitchhiker guide to: Secant varieties and tensor decomposition. *Mathematics* **6** (2018). URL <https://www.mdpi.com/2227-7390/6/12/314>.
- [34] Cirici, J., Salvadó, J. & Taron, J. Characterization of quantum entanglement via a hypercube of segre embeddings. *Quantum Inf. Process.* **20**, 1–23 (2021). URL <https://link.springer.com/article/10.1007/s11128-021-03186-x>.
- [35] Ballico, E., Bernardi, A., Carusotto, I., Mazzucchi, S. & Moretti, V. *Quantum Physics and Geometry* (Springer Cham, 2019).
- [36] Draisma, J., Horobet, E., Ottaviani, G., Sturmfels, B. & Thomas, R. R. The euclidean distance degree of an algebraic variety. *Found. Comput. Math.* **16**, 99–149 (2016). URL <https://link.springer.com/article/10.1007/s10208-014-9240-x>.
- [37] Hillar, C. J. & Lim, L.-H. Most tensor problems are NP-hard. *J. ACM* **60** (2013). URL <https://doi.org/10.1145/2512329>.
- [38] Chen, L., Han, L. & Zhou, L. Computing tensor eigenvalues via homotopy methods. *SIAM J. Matrix Anal. Appl.* **37**, 290–319 (2016). URL <https://doi.org/10.1137/15M1010725>.
- [39] Lieven De Lathauwer, B. D. M. & Vandewalle, J. A multilinear singular value decomposition. *SIAM J. Matrix Anal. Appl.* **21**, 1253–1278 (2000). URL <https://doi.org/10.1137/S0895479896305696>.
- [40] Kroonenberg, P. M. & de Leeuw, J. Principal component analysis of three-mode data by means of alternating least squares algorithms. *Psychometrika* **45**, 69–97 (1980). URL <https://doi.org/10.1007/BF02293599>.
- [41] Cleve, R., Ekert, A., Macchiavello, C. & Mosca, M. Quantum algorithms revisited. *Proc. R. Soc. London, Ser. A.* **454**, 339–354 (1998). URL <https://royalsocietypublishing.org/doi/10.1098/rspa.1998.0164>.
- [42] Regalia, P. & Kofidis, E. The higher-order power method revisited: convergence proofs and effective initialization. *Proceedings of the Acoustics, Speech, and Signal Processing* **5**, 2709–2712 (2000). URL <https://ieeexplore.ieee.org/document/861047>.
- [43] Uschmajew, A. A new convergence proof for the higher-order power method

- and generalizations. *Pac. J. Optim.* **11**, 309–321 (2015). URL http://manu71.magtech.com.cn/Jwk3_pjo/EN/Y2015/V11/I2/309#3.
- [44] Hu, S. & Li, G. Convergence rate analysis for the higher order power method in best rank one approximations of tensors. *Numer. Math.* **140**, 993–1031 (2018).
- [45] Qiskit contributors. Qiskit: An open-source framework for quantum computing (2023).
- [46] Yoshioka, N. *et al.* Diagonalization of large many-body hamiltonians on a quantum processor. *Arxiv* (2024). URL <https://arxiv.org/pdf/2407.14431>.
- [47] Vovrosh, J. *et al.* Simple mitigation of global depolarizing errors in quantum simulations. *Phys. Rev. E* **104**, 035309 (2021). URL <https://link.aps.org/doi/10.1103/PhysRevE.104.035309>.
- [48] Denkert, C., Cleve, R., Emerson, J. & Livine, E. Exact and approximate unitary 2-designs and their application to fidelity estimation. *Physical Review A* **80**, 012304 (2009). URL <https://journals.aps.org/pr/abstract/10.1103/PhysRevA.80.012304>.
- [49] Emerson, J., Alicki, R. & Życzkowski, K. Scalable noise estimation with random unitary operators. *J. Opt. B: Quantum Semiclass. Opt* **7**, S347–S352 (2005).
- [50] Kolda, T. G. & Mayo, J. R. Shifted power method for computing tensor eigenpairs. *SIAM Journal on Matrix Analysis and Applications* **32**, 1095–1124 (2011). URL <https://doi.org/10.1137/100801482>.
- [51] Streltsov, A., Kampermann, H. & Bruß, D. Linking a distance measure of entanglement to its convex roof. *New J. Phys.* **12**, 2–18 (2010). URL <https://dx.doi.org/10.1088/1367-2630/12/12/123004>.
- [52] Nielsen, M. A. & Chuang, I. L. *Quantum Computation and Quantum Information* (Cambridge University Press, 2010).
- [53] Zhou, Y., Wilkinson, D., Schreiber, R. & Pan, R. Fleischer, R. & Xu, J. (eds) *Large-Scale Parallel Collaborative Filtering for the Netflix Prize*. (eds Fleischer, R. & Xu, J.) *Algorithmic Aspects in Information and Management*, 337–348 (Springer, Berlin, Heidelberg, 2008).
- [54] Xu, Z. & Li, P. Wallach, H. *et al.* (eds) *Towards practical alternating least-squares for CCA*. (eds Wallach, H. *et al.*) *Advances in Neural Information Processing Systems*, Vol. 32 (Curran Associates, Inc., 2019). URL https://proceedings.neurips.cc/paper_files/paper/2019/file/af3b6a54e9e9338abc54258e3406e485-Paper.pdf.

Supplementary Materials

A.1 Implementation of Gauss-Seidel method and Shifted HOPM algorithms

The approach presented in this paper allows us to also implement the Gauss-Seidel method (GSM), which (as authors of the work [29] claim) should converge to the global minimum with higher probability. The difference with HOPM is in line 6 of Algorithm 1: it is changed to

$$\mathbf{v}_i^{(k+1)} = \lambda^{(k)} \psi \times_i \left(\mathbf{v}_1^{(k+1)*}, \dots, \mathbf{v}_{i-1}^{(k+1)*}, \mathbf{v}_{i+1}^{(k)*}, \dots, \mathbf{v}_n^{(k)*} \right) + \beta \mathbf{v}_i^{(k)}, \quad (28)$$

where $0 < \beta \in \mathbb{R}$ is a free parameter of the algorithm.

To implement GSM the only change to our algorithm is in the classical step where we recover the angles $(\check{\vartheta}_i^{(k+1)}, \check{\varphi}_i^{(k+1)})$ using one-qubit tomography. Instead of Eq. (10) we need to solve the following system of equations to find $(\vartheta_i^{(k+1)}, \varphi_i^{(k+1)})$,

$$\begin{aligned} A^2 \cos^2 \frac{\vartheta_i^{(k+1)}}{2} &= \left| \lambda^{(k)} e^{-i\check{\varphi}_i^{(k+1)}/2} \cos \frac{\check{\vartheta}_i^{(k+1)}}{2} + \beta e^{-i\varphi_i^{(k)}/2} \cos \frac{\vartheta_i^{(k)}}{2} \right|^2; \\ A^2 \sin \vartheta_i^{(k+1)} \sin \varphi_i^{(k+1)} &= (\lambda^{(k)})^2 \sin \check{\vartheta}_i^{(k+1)} \sin \check{\varphi}_i^{(k+1)} \\ &\quad + \beta^2 \sin \vartheta_i^{(k)} \sin \varphi_i^{(k)} + 2\beta \lambda^{(k)} \sin \frac{\check{\vartheta}_i^{(k+1)} + \vartheta_i^{(k)}}{2} \sin \frac{\check{\varphi}_i^{(k+1)} + \varphi_i^{(k)}}{2}; \\ A^2 \sin \vartheta_i^{(k+1)} \cos \varphi_i^{(k+1)} &= (\lambda^{(k)})^2 \sin \check{\vartheta}_i^{(k+1)} \cos \check{\varphi}_i^{(k+1)} \\ &\quad + \beta^2 \sin \vartheta_i^{(k)} \cos \varphi_i^{(k)} + 2\beta \lambda^{(k)} \sin \frac{\check{\vartheta}_i^{(k+1)} + \vartheta_i^{(k)}}{2} \cos \frac{\check{\varphi}_i^{(k+1)} + \varphi_i^{(k)}}{2}, \end{aligned} \quad (29)$$

where

$$A^2 = (\lambda^{(k)})^2 + \beta^2 + 2\beta \lambda^{(k)} \cos \frac{\check{\vartheta}_i^{(k+1)} - \vartheta_i^{(k)}}{2} \cos \frac{\check{\varphi}_i^{(k+1)} - \varphi_i^{(k)}}{2}$$

is a normalization coefficient.

Note, that GSM is similar to the so-called shifted HOPM (SHOPM) algorithm [50, 27], with the only difference being that SHOPM does not have the current eigenvalue estimate $\lambda^{(k)}$ as a prefactor on the right-hand side of Eq. (28). Thus to get the SHOPM quantum-classical hybrid implementation one needs to set $\lambda^{(k)}$ in Eq. (29) to one.

A.2 Supplemental simulation results

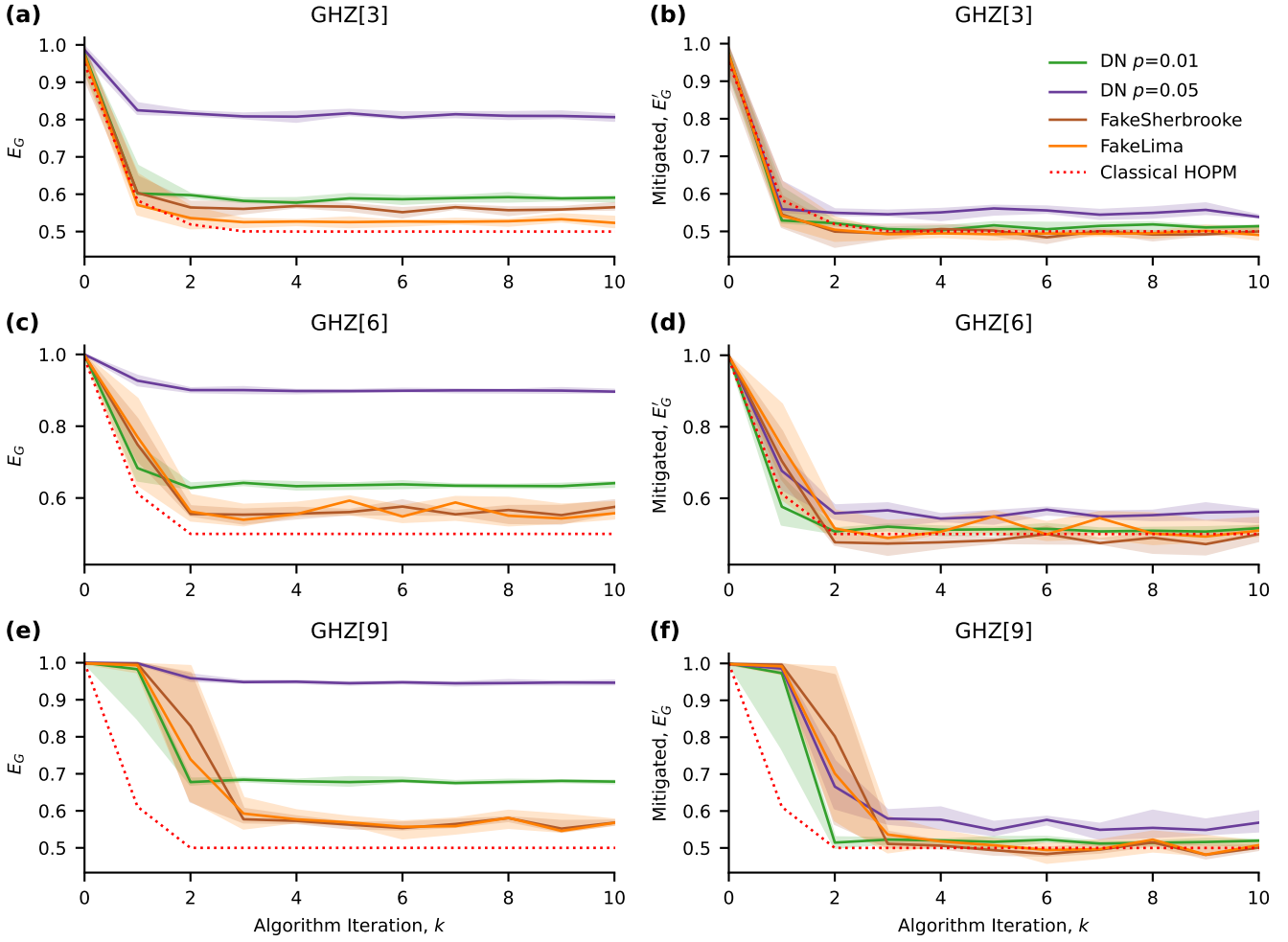


Fig. 7: Simulation and mitigation results for the QHOPM algorithm on GHZ states. Row (a) (b) show GHZ[3], (c) (d) show GHZ[6], (e) (f) show GHZ[9]. Column (a) (c) (e) shows the effect of noise on convergence. Column (b) (d) (f) shows the effects of mitigation on the noisy simulation. Each simulation was run 10 times (with the same 10 random initial separable states) with 1×10^5 shots per each measurement. Solid lines represent the mean geometric entanglement, E_G , and the lightly shaded colours represent the standard deviation. The colour of the lines represents the noise model used for the simulation (see legend). Red dotted lines show results of classical HOPM.

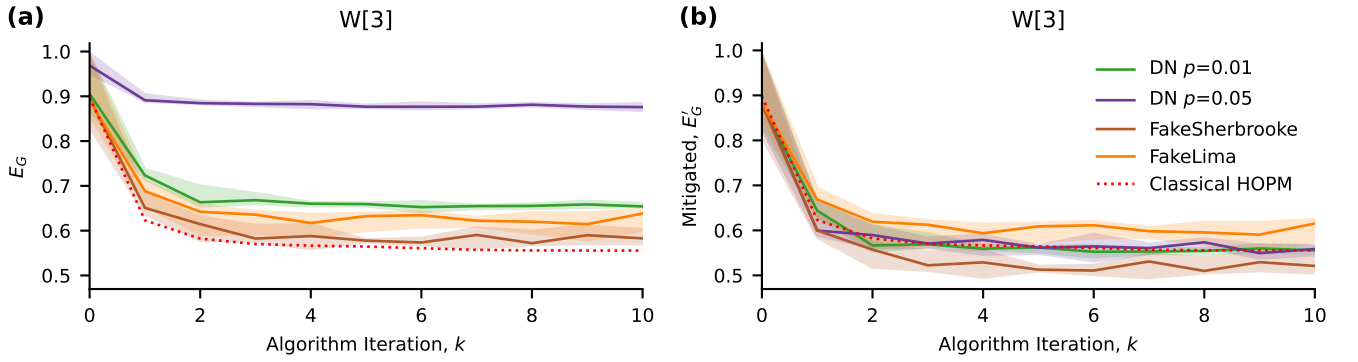


Fig. 8: Simulation and mitigation results for the QHOPM algorithm on the $W[3]$ state. (a) shows the effect of noise on convergence. (b) shows the effects of mitigation on the noisy simulation. $\hat{E}_G = 5/9 \approx 0.554$. Each simulation was run 10 times (with the same 10 random initial separable states) with 1×10^5 shots per each measurement. Solid lines represent the mean geometric entanglement, E_G , and the lightly shaded colours represent the standard deviation. The colour of the lines represents the noise model used for the simulation (see legend). Red dotted lines show results of classical HOPM.

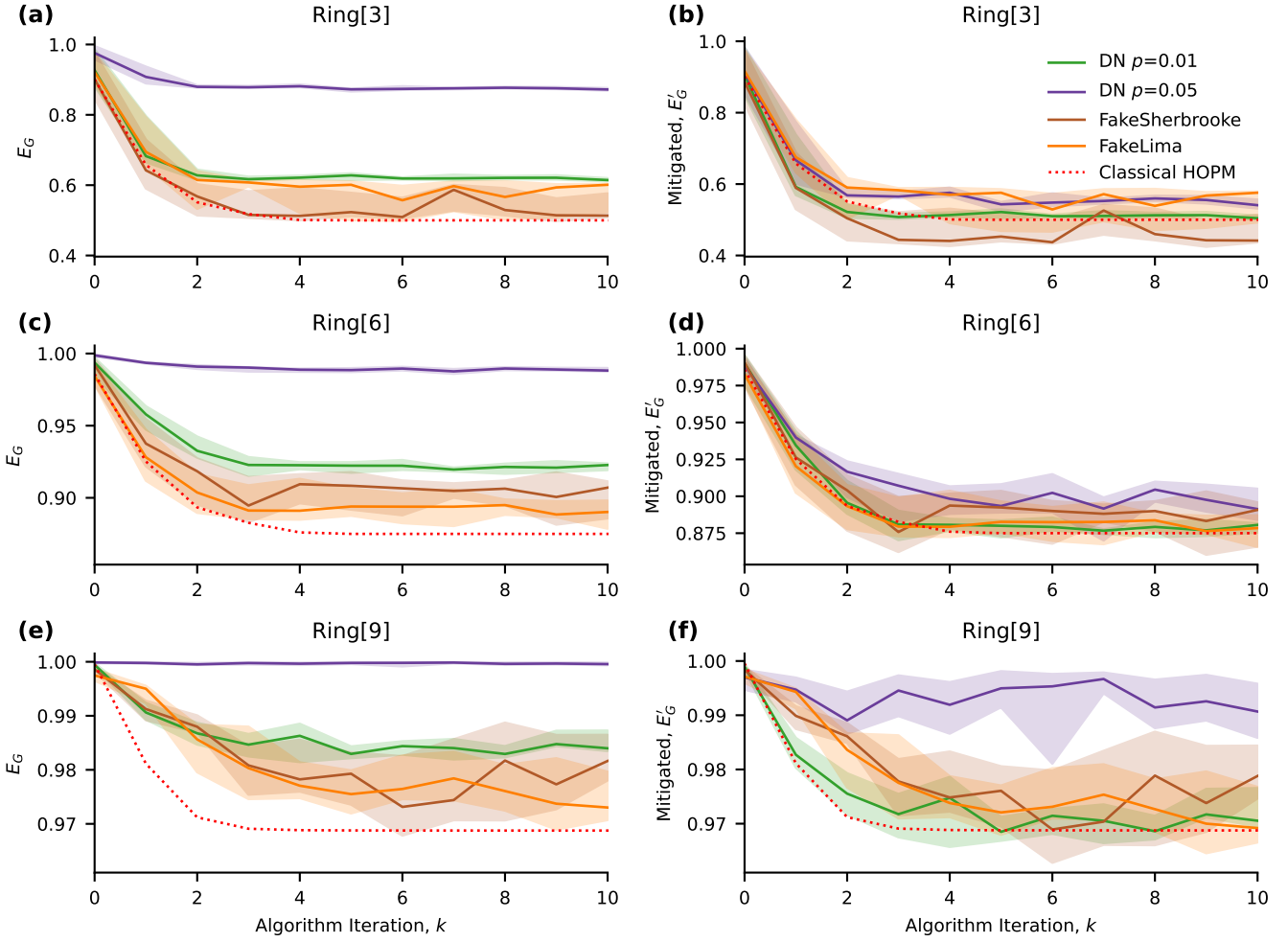


Fig. 9: Simulation and mitigation results for the QHOPM algorithm on Ring states. Row (a) (b) show Ring[3], (c) (d) show Ring[6], (e) (f) show Ring[9]. Column (a) (c) (e) shows the effect of noise on convergence. Column (b) (d) (f) shows the effects of mitigation on the noisy simulation. Each simulation was run 10 times (with the same 10 random initial separable states) with 1×10^5 shots per each measurement. Solid lines represent the mean geometric entanglement, E_G , and the lightly shaded colours represent the standard deviation. The colour of the lines represents the noise model used for the simulation (see legend). Red dotted lines show results of classical HOPM.

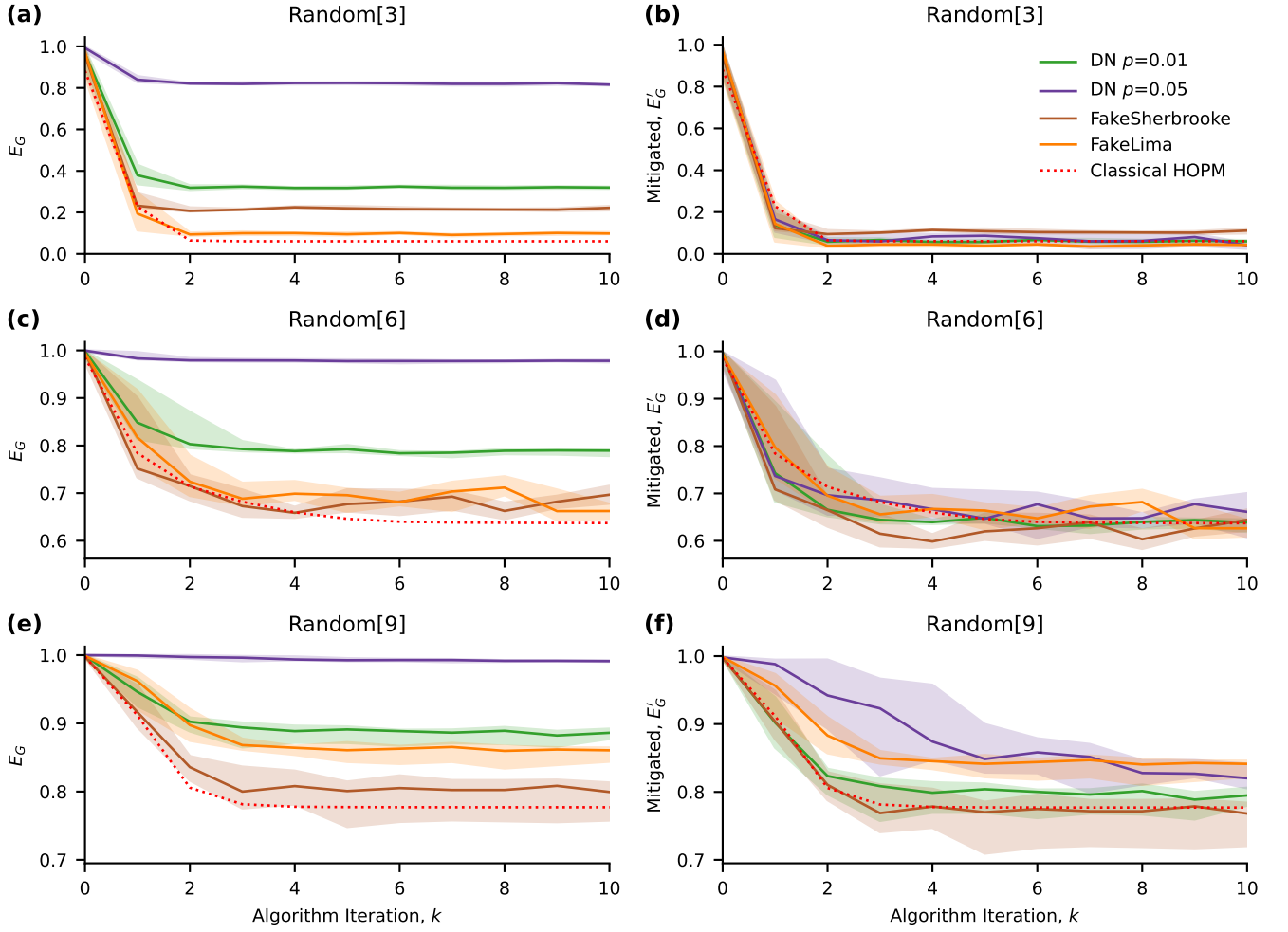


Fig. 10: Simulation and mitigation results for the QHOPM algorithm on Random states. Row (a) (b) show Random[3], (c) (d) show Random[6], (e) (f) show Random[9]. Column (a) (c) (e) shows the effect of noise on convergence. Column (b) (d) (f) shows the effects of mitigation on the noisy simulation. Each simulation was run 10 times (with the same 10 random initial separable states) with 1×10^5 shots per each measurement. Solid lines represent the mean geometric entanglement, E_G , and the lightly shaded colours represent the standard deviation. The colour of the lines represents the noise model used for the simulation (see legend). Red dotted lines show results of classical HOPM.